

Reducing Effective System Dimensionality with Long-Range Collective Dipole-Dipole Interactions

Ashwin K. Boddeti^{1,2}, Yi Wang³, Xitlali G. Juarez⁴, Alexandra Boltasseva^{1,2}, Teri W. Odom^{3,4,5}, Vladimir Shalaev^{1,2}, Hadiseh Alaeian^{1,2,6}, and Zubin Jacob^{1,2,*}

¹Elmore Family School of Electrical and Computer Engineering, Purdue University, West Lafayette, Indiana 47907, USA

²Birck Nanotechnology Center, Purdue University, West Lafayette, Indiana 47907, USA

³Graduate Program in Applied Physics, Northwestern University, Evanston, Illinois 60208, USA

⁴Department of Materials Science and Engineering, Northwestern University, Evanston, Illinois 60208, USA

⁵Department of Chemistry, Northwestern University, Evanston, Illinois 60208, USA

⁶School of Physics and Astronomy, Purdue University, West Lafayette, Indiana 47907, USA



(Received 4 May 2023; accepted 14 March 2024; published 25 April 2024)

Dimensionality plays a crucial role in long-range dipole-dipole interactions (DDIs). We demonstrate that a resonant nanophotonic structure modifies the apparent dimensionality in an interacting ensemble of emitters, as revealed by population decay dynamics. Our measurements on a dense ensemble of interacting quantum emitters in a resonant nanophotonic structure with long-range DDIs reveal an effective dimensionality reduction to $\bar{d} = 2.20(12)$, despite the emitters being distributed in 3D. This contrasts with the homogeneous environment, where the apparent dimension is $\bar{d} = 3.00$. Our work presents a promising avenue to manipulate dimensionality in an ensemble of interacting emitters.

DOI: 10.1103/PhysRevLett.132.173803

Introduction.—In a dense ensemble of interacting emitters, each emitter perceives the other neighboring emitters via position-dependent dipole-dipole interactions (DDIs). The role of geometry in such position-dependent collective interactions between an ensemble of emitters has been of fundamental interest [1–7]. Controlling the dimensionality is appealing as a lower-dimensional emitter geometry shows strong quantum fluctuations [8]. This can potentially provide a host of benefits in realizing platforms to probe long-range interactions [1,2], quantum phases such as quantum spin liquids [3,4], transient super solid behavior [5], and quantum phase transition in transverse Ising models [9], in addition to providing an advantage in quantum sensing applications, mitigating decoherence [1,5], and in long-range energy transport of delocalized excitons [7]. More recently, interesting physical effects on Dicke superradiance in 1D, 2D, and 3D arrays of atoms have been theoretically predicted [6]. Thus, realizing a lower-dimensional system supporting long-range DDIs is of significant importance.

While 1D and 2D interacting ensembles of emitters have been realized in cold-atom systems, it remains largely unexplored in solid-state platforms. Only recent efforts demonstrating a thin layer of emitters (spin 1 nitrogen vacancy (NV) centres and spin 1/2 substitutional nitrogen (P1) centres) have paved the way for realizing lower-dimensional systems in solid states [1,2]. The P1 system's many-body noise is characterized by the decoherence of NV center probe spins and shows stretched exponential decay dynamics [1].

As DDIs are mediated by the underlying electromagnetic fields, tailoring them provides an alternative route to manipulate the apparent dimensionality. Recently, interfacing quantum emitters with light within nanophotonic structures has provided the means to control and study collective DDIs [10]. This led to the demonstration of long-range resonance energy transfer in incoherent systems [11,12], and sub- and superradiant emission dynamics in coherent systems [13–16].

Here we modify the apparent dimensionality using a nanophotonic structure that supports dispersive delocalized resonant modes that mediate the interactions. These modes lead to modification of the spatial distribution of the perceived neighboring emitters. We experimentally probe the apparent dimensionality of the interacting ensemble of donor and acceptor emitters, encoded in the interacting emitters' temporal decay dynamics. While individual emitters decay exponentially, the lifetime decay dynamics of an interacting ensemble of emitters follow a stretched exponential decay, revealing a noninteger power β in time,

$$I(t)/I_0 = \exp(-\gamma_D t) \exp(-\alpha t^\beta), \quad (1)$$

where γ_D is the spontaneous decay rate and α is the effective interaction volume [17–19]. The noninteger power, β , originates due to DDIs between the emitters and captures the apparent dimensionality sensed by the mutually interacting emitters,

$$\beta = \bar{d}/S, \quad (2)$$

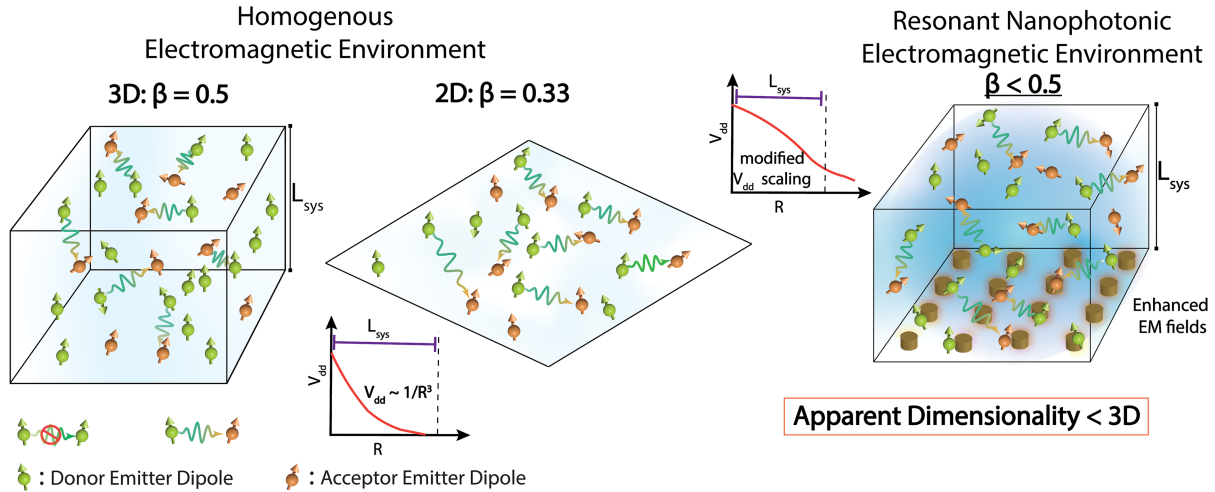


FIG. 1. Concept of apparent dimensionality of an interacting ensemble of emitters. The apparent dimensionality is related to the noninteger exponent of time in the fluorescence decay dynamics $I(t)/I_0 = \exp(-\gamma_D t) \exp(-\alpha t^\beta)$. In a homogeneous environment, $\beta = 0.5$ (0.33) for the 3D (2D) spatial distribution of emitters. A resonant nanophotonic environment modifies the spatial distribution of the neighboring emitters sensed by each interacting emitter which results in the modification of the temporal decay dynamics. This reduces the apparent dimensionality experienced by the interacting emitters, which is reflected in the noninteger exponent, $\beta < 0.5$, though, the emitters are distributed in a 3D volume. The green dipoles represent the donor emitters and the orange represents acceptor emitters.

where \bar{d} is the apparent dimension, and $S = 6$ for electric DDIs [18]. Such relaxation decay dynamics arising due to DDIs are common in other systems such as the kinetic Ising model below the critical temperature, an interacting ensemble of spins [1], in ultracold atoms, and in ions [20–25]. The underlying physics that governs DDIs is universal; here, we focus on DDIs at room temperature, where it is difficult to discern coherent effects.

The two underlying characteristics that relate to this intriguing noninteger power, β in the decay dynamics (and thus the apparent dimensionality) are (i) the distance scaling law associated with DDIs in the vicinity of a nanophotonic environment and (ii) the competition between the characteristic DDI length scale R_0 and the system size L_{sys} . The interplay between these two characteristic lengths determines the spatial extent of the emitters sensed by each donor quantum emitter. Figure 1 conceptually shows the origin of the reduced apparent dimensionality. In homogeneous environments, the DDI potential, V_{dd} , scales as $\sim 1/R^3$. For timescales beyond the coherence times of the interacting system (i.e., the emitters do not possess memory of previous interaction events), the noninteger power, $\beta = 1/2$ (1/3) for the three-dimensional (two-dimensional) spatial distribution of emitters [12] for timescales beyond the coherence times of the interacting system (i.e., the emitters do not possess memory of previous interaction events). See Supplementary Material for more information [12,19,26–33].

In contrast to homogeneous environments, a resonant nanophotonic structure modifies the strength, range, and characteristic interaction length scale of DDIs

[11,12,14,34,35]. Because of this modification of underlying electromagnetic fields, an ensemble of interacting quantum emitters coupled to such resonant nanophotonic structures perceive a modified spatial distribution of emitters. Thus, the spatial extent, strength, and confinement of electromagnetic fields, the hierarchy of distances (and thus the DDI strength) averaging over all possible sites of the interacting emitters is modified. This leads to a modification in the temporal decay dynamics which is reflected in the noninteger exponent β and hence the apparent dimensionality of the interacting system.

System.—In this study, we consider the interaction of an ensemble of donor (Alq_3) and acceptor (R6G) emitters in both resonant and off-resonant nanophotonic structures. The dipole-dipole interactions (DDIs) between the emitters lead to resonance energy transfer. The DDI potential is related to the dyadic Green's function, $V_{dd}(\mathbf{r}_A, \mathbf{r}_D; \omega_D) = -(\omega_D^2/\epsilon_0 c^2) \mathbf{n}_A \cdot \bar{\mathbf{G}}(\mathbf{r}_A, \mathbf{r}_D; \omega_D) \cdot \mathbf{n}_D$, where \mathbf{r}_A and \mathbf{r}_D are the positions of the acceptor and donor emitters, respectively, \mathbf{n}_A and \mathbf{n}_D are unit orientation vectors of the acceptor and donor emitters, respectively, ω_D is the radial frequency of the donor emitter, ϵ_0 is vacuum permittivity, and c is the speed of light [12,34]. The interaction strength is proportional to the rate of energy transfer, $\Gamma_{ET}(\mathbf{r}_A, \mathbf{r}_D; \omega_D) = (2\pi/\hbar^2) |V_{dd}(\mathbf{r}_A, \mathbf{r}_D; \omega_D)|^2 f_D(\omega_D) \sigma_A(\omega_D)$, where $f_D(\omega_D)$ and $\sigma_A(\omega_D)$ are the emission spectra of the donor emitter and absorption cross section of the acceptor emitter, respectively. Figure 2(a) shows the spectral overlap between the donor emission spectrum (Alq_3), the acceptor absorption spectrum (R6G), and the extinction spectrum of both a resonant and an off-resonant plasmonic lattice. The

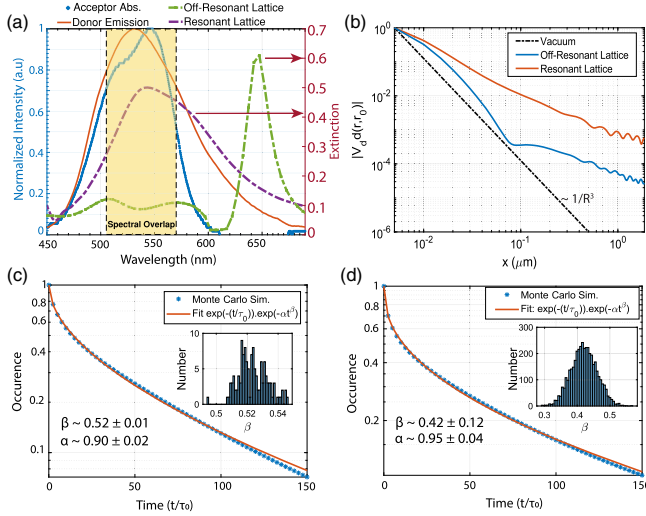


FIG. 2. (a) Acceptor emitter's absorption spectrum (blue curve), donor emitter's emission spectrum (orange curve), extinction spectrum of a resonant plasmonic lattice with lattice constant ~ 300 nm (purple dash curve), and off-resonant plasmonic lattice with lattice constant ~ 350 nm (green dash-dot curve). The extinction spectrum of the resonant plasmonic lattice spectrally overlaps with the emission-absorption spectrum of the donor and acceptor emitters (yellow highlighted region). (b) Calculated dipole-dipole interaction potential $|V_{dd}|$ for the resonant and off-resonant plasmonic lattice. The resonant plasmonic lattice shows a strikingly modified scaling law. (c) Monte Carlo simulations depicting the temporal decay dynamics of donor emitters for $|V_{dd}|^2 = R_0^6/R^6$ scaling and $R_0 \ll L_{\text{sys}}$ with $\beta \sim 0.52$. Inset: values of β for randomized spatial distributions of emitters. (d) Monte Carlo simulations showing the temporal decay dynamics of donor emitters for $R_0 \sim L_{\text{sys}}$. The reduced dimensionality is evident from the estimated values of $\beta \sim 0.4$. Inset: values of β for randomized spatial distributions of emitters.

resonant plasmonic lattice modes mediate the DDIs between the donor and acceptor emitters. The resonant plasmonic lattice modifies the scaling, strength, and range of the DDI potential $|V_{dd}|$ as shown in Fig. 2(b). The scaling of the DDI potential $|V_{dd}|$ is significantly modified with distance $R = |\mathbf{r}_D - \mathbf{r}_A|$ in a resonant structure, whereas the DDI potential decays rapidly with distance in an off-resonant plasmonic lattice. The resonances of the plasmonic lattice modes can be tuned by altering the lattice constant.

The relaxation dynamics of the interacting ensemble of donor-acceptor emitters are governed by nonlinear coupled rate equations (see Supplemental Material) [26]. Here the Monte Carlo simulation method is employed to estimate the temporal decay dynamics of the donor emitters (see Supplemental Material) [26]. Figure 2(c) shows the estimated temporal decay dynamics for homogenous environments, i.e., $R_0 \ll L_{\text{sys}}$, where noninteger exponent is $\beta \sim 0.52$. This is commensurate to a three-dimensional interacting system and matches well with the predicted

theoretical value (see derivation in Supplemental Material) [26]. The inset shows the estimated values of β for various runs of the Monte Carlo simulations with different random spatial distributions of the emitters. On the other hand when $R_0 \sim L_{\text{sys}}$ as shown in Fig. 2(d), the value of the noninteger exponent is $\beta \sim 0.42(12)$. This is commensurate to an effective dimension of $\bar{d} \sim 2.50(72)$ —lower than a three-dimensional system. The inset shows the broad distribution in the values of β with a standard deviation of ~ 0.12 for 1024 different iterations of the Monte Carlo simulation.

In practice, a resonant plasmonic lattice aids in realizing an apparent lower-dimensional system. The modified scaling of the DDI potential, $|V_{dd}|$ coupled with increased interaction strength, leads to an increase in the characteristic interaction length scale R_0 . Under certain conditions when the system size, i.e., the spatial extent of emitters, L_{sys} becomes comparable to the R_0 in addition to the scaling law, the interacting system of emitters (in resonant nanophotonic structures) perceive an apparent lower dimension. We explore this effect here to engineer the dimensionality of collective (many-dipole) DDIs.

Experiment.—To elucidate this, in the experiment, we measure the fluorescence lifetime decay trace of the interacting emitters in both resonant and off-resonant nanophotonic structures. The dye molecules Alq₃ (0.83 mM) and R6G (0.25 mM) are embedded in polymethyl methacrylate polymer thin films on the aforementioned samples. We use a time-correlated single-photon counting technique with a narrow-band filter [520(5) nm] centered at the peak emission of the donor emitter to measure the fluorescence lifetime decay traces (see Supplemental Material [26]). Figure 3 shows the measured lifetime decay when the interacting emitters embedded in different nanophotonic structures such as (i) glass substrate (i.e., a homogeneous environment), Fig. 3(a), (ii) a TiO₂ dielectric lattice, Fig. 3(b), (iii) an off-resonant plasmonic lattice, Fig. 3(c), and (iv) a resonant plasmonic lattice, Fig. 3(d). We observe a striking deviation to the noninteger exponent in time from the typical $\beta = 0.5$ in 3D homogeneous environments to $\beta \sim 0.37$ [an effective lower dimension $\bar{d} \sim 2.20(12)$] in a dispersive resonant nanophotonic structure—a plasmonic lattice. We note that this value is close to that of a 2D system. This elucidates that the underlying resonant modes supported by the plasmonic lattice indeed modify the apparent dimension perceived by the interacting ensemble of emitters. The TiO₂ dielectric lattice has the same geometric features as the resonant plasmonic lattice but supports no resonances. The measurements on the TiO₂ lattice help rule out effects due to the underlying geometry of the lattice. On the other hand, the measurements on the off-resonant plasmonic lattice elucidate that the origin of the apparent lower dimension is purely due to the lattice resonance and not from the localized-surface-plasmon resonance of the constituent metal nanoparticles.

The noninteger exponent in time is estimated by fitting the temporal fluorescence decay trace with a Laplace transform

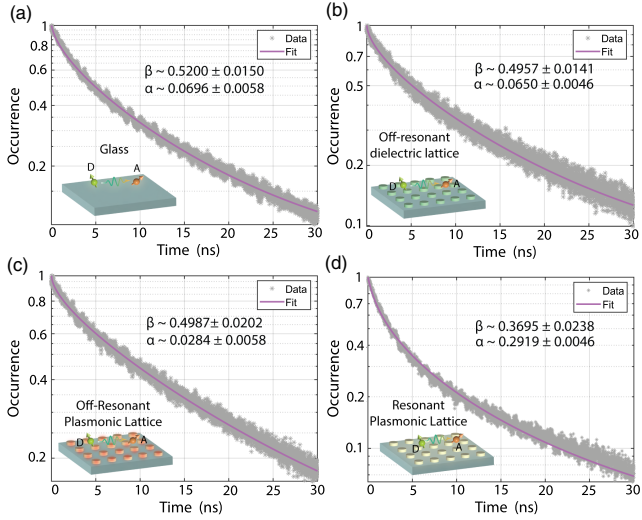


FIG. 3. Measured fluorescence lifetime decay when the interacting emitters are in different electromagnetic environments: (a) glass substrate (i.e., a homogeneous environment), (b) TiO_2 dielectric lattice (i.e., an off-resonant inhomogeneous electromagnetic environment), and (c) a plasmonic lattice (i.e., a resonant inhomogeneous electromagnetic environment). The value of $\beta \sim 0.5$ in both inhomogeneous and off-resonant inhomogeneous environments. This is commensurate with a 3D system. In contrast, the faster-than-exponential decay dynamics on a resonant silver (Ag) plasmonic lattice reveals an exponent value of ~ 0.37 . This is commensurate to an effective lower dimension $\bar{d} \sim 2.20(12)$. The emitters were embedded in $\sim 1 \mu\text{m}$ thick polymer thin films.

of an underlying probability density function [29],

$$\frac{I(t)}{I_0} = \int_0^\infty G_\delta(\gamma) e^{-\gamma t} d\gamma \int_0^\infty H_\beta(\Gamma_{ET}) e^{-\Gamma_{ET} t} d\Gamma_{ET}. \quad (3)$$

In Eq. (3), the first term is associated with the spontaneous decay of donor emitters, while the second term is associated with resonance energy transfer (DDIs). $G_\delta(\gamma)$ is the probability density function (PDF) associated with the distribution of spontaneous emission decay rates, and $H_\beta(\Gamma_{ET})$ is the PDF for resonant energy transfer rates. For a homogeneous environment, with no significant enhancement in the local density of optical states (LDOS), $G_\delta(\gamma) = \delta(\gamma - \gamma_D)$, where $\delta(\gamma - \gamma_D)$ is the delta function, and γ_D is the decay rate of the individual donor emitter. In contrast, in an inhomogeneous environment, each donor experiences different LDOS and, thus, different spontaneous emission decay rates [36]. As the DDI in this particular scenario is a weak perturbation, the spontaneous decay rate of the donors is estimated from the fluorescence decay trace of donors in the absence of the acceptor emitter (see Supplemental Material). The PDF of resonance energy transfer rates $H_\beta(\Gamma_{ET})$ is estimated by fitting the fluorescence lifetime decay trace with the spontaneous decay rate PDF $G_\delta(\gamma)$ as a fixed parameter. The underlying probability distributions have a

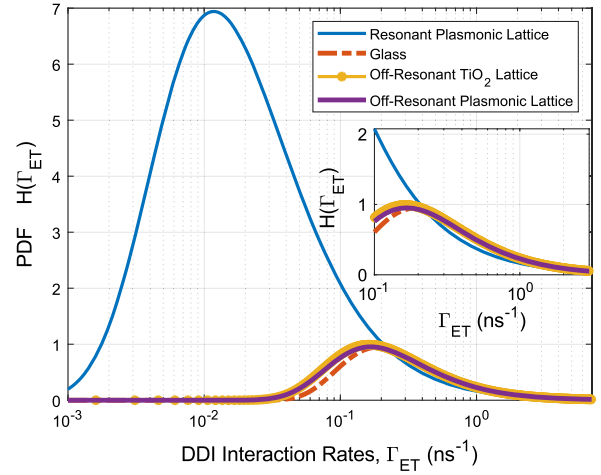


FIG. 4. Extracted probability density function for the resonance energy transfer rate on various electromagnetic environments: (i) glass, a homogeneous environment (dash-dot red curve), (ii) an inhomogeneous environment, TiO_2 nanoparticle lattice having the same lattice constant and dimensions as the resonant plasmonic lattice (dotted yellow curve), (iii) an off-resonant plasmonic lattice (purple curve), and (iv) a resonant plasmonic lattice (blue curve). The PDF of the energy transfer rates on the resonant plasmonic lattice is not only shifted but also broader. Inset: reduced number of events having stronger interaction strength (in the tail).

characteristic long-tail behavior and are related to Lévy stable distributions [28].

Figure 4 shows the extracted PDF of the resonant energy transfer rate (Γ_{ET}) distribution. The PDFs obtained in the resonant inhomogeneous environment are observed to differ from those in the homogeneous and off-resonant inhomogeneous environments. This directly indicates that the sensed spatial distribution of emitters is modified. As the plasmonic lattice supports dispersive delocalized resonant modes that can mediate interactions between the donor and acceptor emitters over larger distances, the underlying PDFs show a broader distribution of rates. Furthermore, the number of interaction events in the tail of the distribution reduces, which indicates a reduction in the total number of larger magnitude DDI interaction strengths, Γ_{ET} ; see inset of Fig. 4. The plasmonic lattice shows a higher probability of lower DDI rates. This result may appear counterintuitive, as the plasmonic lattice enhances the DDI rates overall. The plasmonic lattice enhances the interactions at larger distances, i.e., beyond the Förster resonance energy transfer radius. The experiments were performed at densities wherein the mean-nearest neighbor separation between the interacting pair of emitters is $\sim 5\text{--}10 \text{ nm}$. At these distances, $\sim 1/r^6$ is more dominant than the scaling arising due to the plasmonic lattice, thus the DDI rates are lower on the plasmonic lattice. The strength of interactions gets enhanced at larger distances as shown in a previous work [12]. See Supplemental Material for more details.

Conclusion.—In summary, we experimentally demonstrated that the apparent dimensionality of an interacting ensemble of emitters could be modified using a resonant nanophotonic structure. The temporal fluorescence decay dynamics show a noninteger exponent β that relates to the apparent dimensionality of the interacting system. The value of apparent dimensionality on a resonant plasmonic lattice shows a stark contrast value of $\bar{d} \sim 2.20(12)$, in comparison to $\bar{d} \sim 3.0$ obtained on glass, an off-resonant TiO_2 dielectric lattice, and an off-resonant plasmonic lattice. Further, we extract the underlying distribution of energy transfer rates for the emitters' interacting ensemble, indicating that the interacting emitters' perceived apparent dimensionality is modified. This arises due to modifying the underlying distribution of energy transfer rates. This work paves the way for engineering interacting systems with apparent lower dimensionality. Though the presented results are semiclassical and discernible coherent effects cannot be observed at room temperatures, they can readily be applied to regimes where quantum effects are more prominent such as in ultracold atoms [14], solid-state emitters systems [1,2], rare-earth ions [37,38], Rydberg excitons in solids [39], and quantum-dots systems [13]. Such nanophotonic structures can potentially provide an alternative route to realize two-dimensional systems that host new quantum many-body phases, help mitigate decoherence for quantum sensing, memories, and quantum network applications, realize novel, more efficient light-harvesting systems, and potentially improve biological samples imaging.

This work was supported by the U.S. Department of Energy (DOE), Office of Basic Sciences under DE-SC0017717 (A. K. B., A. B., V. S., and Z. J.), IUCRC at the U.S. National Science Foundation under Grant No. 2224960, and the Air Force Office of Scientific Research under Grant No. FA9550-23-1-0489 (H. A.), the Office of Naval Research (ONR) under ONR N00014-21-1-2289 (Y. W. and T. W. O.) and the National Science Foundation under DMR-2207215 and DMR-1904385 (X. G. J. and T. W. O.). This work made use of the NUFAB and EPIC facilities of Northwestern University's NUANCE Center, which has received support from the SHyNE Resource (NSF ECCS-2025633), the IIN, and Northwestern's MRSEC program (NSF DMR-1720139).

- [2] B. L. Dwyer, L. V. Rodgers, E. K. Urbach, D. Bluvstein, S. Sangtawesin, H. Zhou, Y. Nassab, M. Fitzpatrick, Z. Yuan, K. De Greve *et al.*, Probing spin dynamics on diamond surfaces using a single quantum sensor, *PRX Quantum* **3**, 040328 (2022).
- [3] C. Broholm, R. Cava, S. Kivelson, D. Nocera, M. Norman, and T. Senthil, Quantum spin liquids, *Science* **367**, eaay0668 (2020).
- [4] N. Y. Yao, M. P. Zaletel, D. M. Stamper-Kurn, and A. Vishwanath, A quantum dipolar spin liquid, *Nat. Phys.* **14**, 405 (2018).
- [5] L. Chomaz, D. Petter, P. Ilzhöfer, G. Natale, A. Trautmann, C. Politi, G. Durastante, R. Van Bijnen, A. Patscheider, M. Sohmen *et al.*, Long-lived and transient supersolid behaviors in dipolar quantum gases, *Phys. Rev. X* **9**, 021012 (2019).
- [6] E. Sierra, S. J. Masson, and A. Asenjo-Garcia, Dicke superradiance in ordered lattices: Dimensionality matters, *Phys. Rev. Res.* **4**, 023207 (2022).
- [7] B. Wittmann, F. A. Wenzel, S. Wiesneth, A. T. Haedler, M. Drechsler, K. Kreger, J. Köhler, E. W. Meijer, H.-W. Schmidt, and R. Hildner, Enhancing long-range energy transport in supramolecular architectures by tailoring coherence properties, *J. Am. Chem. Soc.* **142**, 8323 (2020).
- [8] R. Samajdar, W. W. Ho, H. Pichler, M. D. Lukin, and S. Sachdev, Complex density wave orders and quantum phase transitions in a model of square-lattice Rydberg atom arrays, *Phys. Rev. Lett.* **124**, 103601 (2020).
- [9] M. Schmitt, M. M. Rams, J. Dziarmaga, M. Heyl, and W. H. Zurek, Quantum phase transition dynamics in the two-dimensional transverse-field Ising model, *Sci. Adv.* **8**, eabl6850 (2022).
- [10] D. E. Chang, J. S. Douglas, A. González-Tudela, C.-L. Hung, and H. J. Kimble, Colloquium: Quantum matter built from nanoscopic lattices of atoms and photons, *Rev. Mod. Phys.* **90**, 031002 (2018).
- [11] W. D. Newman, C. L. Cortes, A. Afshar, K. Cadien, A. Meldrum, R. Fedosejevs, and Z. Jacob, Observation of long-range dipole-dipole interactions in hyperbolic metamaterials, *Sci. Adv.* **4**, eaar5278 (2018).
- [12] A. K. Boddeti, J. Guan, T. Sentz, X. Juarez, W. Newman, C. Cortes, T. W. Odom, and Z. Jacob, Long-range dipole-dipole interactions in a plasmonic lattice, *Nano Lett.* **22**, 22 (2021).
- [13] A. Tirnov, V. Angelopoulou, C. J. van Diepen, B. Schriniski, O. A. D. Sandberg, Y. Wang, L. Midolo, S. Scholz, A. D. Wieck, A. Ludwig *et al.*, Collective super- and subradiant dynamics between distant optical quantum emitters, *Science* **379**, 389 (2023).
- [14] A. Skljarov, H. Kübler, C. S. Adams, T. Pfau, R. Löw, and H. Alaeian, Purcell-enhanced dipolar interactions in nanostructures, *Phys. Rev. Res.* **4**, 023073 (2022).
- [15] A. Goban, C.-L. Hung, J. D. Hood, S.-P. Yu, J. A. Muniz, O. Painter, and H. J. Kimble, Superradiance for atoms trapped along a photonic crystal waveguide, *Phys. Rev. Lett.* **115**, 063601 (2015).
- [16] J. D. Hood, A. Goban, A. Asenjo-Garcia, M. Lu, S.-P. Yu, D. E. Chang, and H. Kimble, Atom-atom interactions around the band edge of a photonic crystal waveguide, *Proc. Natl. Acad. Sci. U.S.A.* **113**, 10507 (2016).

*zjacob@purdue.edu; www.electrodynamics.org

[1] E. J. Davis, B. Ye, F. Machado, S. A. Meynell, W. Wu, T. Mittiga, W. Schenken, M. Joos, B. Kobrin, Y. Lyu, Z. Wang, D. Bluvstein, S. Choi, C. Zu, A. C. B. Jayich, and N. Y. Yao, Probing many-body dynamics in a two-dimensional dipolar spin ensemble, *Nat. Phys.* **19**, 836 (2023).

- [17] T. Förster, Experimentelle und theoretische untersuchung des zwischenmolekularen übergangs von elektronenenergiedifferenzenergie, *Z. Naturforsch. A* **4**, 321 (1949).
- [18] J. Drake, J. Klafter, and P. Levitz, Chemical and biological microstructures as probed by dynamic processes, *Science* **251**, 1574 (1991).
- [19] L. Klushin and O. Tcherkasskaya, Effects of molecular distribution on the fluorescence transfer: Exact results for slab geometry, *J. Chem. Phys.* **119**, 3421 (2003).
- [20] B. Neyenhuis, J. Zhang, P. W. Hess, J. Smith, A. C. Lee, P. Richerme, Z.-X. Gong, A. V. Gorshkov, and C. Monroe, Observation of prethermalization in long-range interacting spin chains, *Sci. Adv.* **3**, e1700672 (2017).
- [21] D. A. Abanin, E. Altman, I. Bloch, and M. Serbyn, Colloquium: Many-body localization, thermalization, and entanglement, *Rev. Mod. Phys.* **91**, 021001 (2019).
- [22] L. Ratschbacher, C. Sias, L. Carcagni, J. M. Silver, C. Zipkes, and M. Köhl, Decoherence of a single-ion qubit immersed in a spin-polarized atomic bath, *Phys. Rev. Lett.* **110**, 160402 (2013).
- [23] H. Takano, H. Nakanishi, and S. Miyashita, Stretched exponential decay of the spin-correlation function in the kinetic Ising model below the critical temperature, *Phys. Rev. B* **37**, 3716 (1988).
- [24] G. Kucsko, S. Choi, J. Choi, P. C. Maurer, H. Zhou, R. Landig, H. Sumiya, S. Onoda, J. Isoya, F. Jelezko *et al.*, Critical thermalization of a disordered dipolar spin system in diamond, *Phys. Rev. Lett.* **121**, 023601 (2018).
- [25] R. Hanson, V. Dobrovitski, A. Feiguin, O. Gywat, and D. Awschalom, Coherent dynamics of a single spin interacting with an adjustable spin bath, *Science* **320**, 352 (2008).
- [26] See Supplemental Material, which includes Refs. [12,27–33], at <http://link.aps.org/supplemental/10.1103/PhysRevLett.132.173803> for analytical derivation for dimensionality in a homogenous environment, relaxation dynamics, Monte Carlo simulation, finite difference time domain simulations, experimental setup, sample fabrication, and the probability density function of resonance energy transfer estimation.
- [27] W. K. Hastings, *Monte Carlo Sampling Methods Using Markov Chains and Their Applications* (Oxford University Press Academic, New York, 1970).
- [28] H. K. Nakamura, M. Sasai, and M. Takano, Scrutinizing the squeezed exponential kinetics observed in the folding simulation of an off-lattice Go-like protein model, *Chem. Phys.* **307**, 259 (2004).
- [29] M. Berberan-Santos, E. Bodunov, and B. Valeur, Mathematical functions for the analysis of luminescence decays with underlying distributions 1. kohlrausch decay function (stretched exponential), *Chem. Phys.* **315**, 171 (2005).
- [30] M. H. Lee, M. D. Huntington, W. Zhou, J.-C. Yang, and T. W. Odom, Programmable soft lithography: Solvent-assisted nanoscale embossing, *Nano Lett.* **11**, 311 (2011).
- [31] J. Henzie, M. H. Lee, and T. W. Odom, Multiscale patterning of plasmonic metamaterials, *Nat. Nanotechnol.* **2**, 549 (2007).
- [32] C. Rackauckas and Q. Nie, DifferentialEquations.jl: A performant and feature-rich ecosystem for solving differential equations in Julia, *J. Open Res. Software* **5**, 15 (2017).
- [33] L. Novotny and B. Hecht, *Principles of Nano-Optics* (Cambridge University Press, Cambridge, England, 2012).
- [34] C. L. Cortes and Z. Jacob, Super-Coulombic atom-atom interactions in hyperbolic media, *Nat. Commun.* **8**, 14144 (2017).
- [35] S.-A. Biehs, V. M. Menon, and G. S. Agarwal, Long-range dipole-dipole interaction and anomalous Förster energy transfer across a hyperbolic metamaterial, *Phys. Rev. B* **93**, 245439 (2016).
- [36] G. M. Akselrod, C. Argyropoulos, T. B. Hoang, C. Ciraci, C. Fang, J. Huang, D. R. Smith, and M. H. Mikkelsen, Probing the mechanisms of large Purcell enhancement in plasmonic nanoantennas, *Nat. Photonics* **8**, 835 (2014).
- [37] A. Ruskuc, C.-J. Wu, J. Rochman, J. Choi, and A. Faraon, Nuclear spin-wave quantum register for a solid-state qubit, *Nature (London)* **602**, 408 (2022).
- [38] M. T. Uysal, M. Raha, S. Chen, C. M. Phenicie, S. Ourari, M. Wang, C. G. Van de Walle, V. V. Dobrovitski, and J. D. Thompson, Coherent control of a nuclear spin via interactions with a rare-earth ion in the solid state, *PRX Quantum* **4**, 010323 (2023).
- [39] T. Kazimierczuk, D. Fröhlich, S. Scheel, H. Stoltz, and M. Bayer, Giant Rydberg excitons in the copper oxide Cu₂O, *Nature (London)* **514**, 343 (2014).